# VLBI Instrumental Effects, Part I

J. W. Layland and W. J. Hurd

Communications Systems Research Section

*Very Long Baseline Interferometry (VLBI) is a method for observation of extra-galactic radio sources which appears to have potential for precise long-distance Earth surveying, clock synchronization and spacecraft navigation. For the past several years, many researchers at JPL and elsewhere have been working to establish the accuracy of VLBI observations. The intent of the work reported here has been to review the principal components of the VLBI instrument in order to estimate and/or bound the systematic error contributions. In this first of a series of articles, we establish the definitions and tools which we need in order to apply filter transfer-function analysis to the VLBI receiver, and we use it to estimate the sensitivity of the VLBI receiver to plausible filter variations.*

## I. Introduction

Very Long Baseline Interferometry (VLBI) is a method for observation of extragalactic radio sources which appears to have potential for precise long-distance Earth surveying, clock synchronization and spacecraft navigation (Ref. 1). For the past several years, many researchers at JPL and elsewhere have been working to establish the accuracy of VLBI observations. The intent of the work reported here has been to review the principal components of the VLBI instrument in order to estimate and/or bound the systematic error contributions. In this first of a series of articles, we establish the definitions and tools which we need in order to apply filter transfer-function analysis to the VLBI receiver, and we use it to estimate the sensitivity of the VLBI receiver to plausible filter variations. We also estimate the error contributions due to uncertainty in modeling of the receiver channels with bandwidth synthesis processing. In the second article of this series, we will estimate

error contributions from channel modeling with full-band sampling.

Section II of this article is an overview description of the VLBI instrument. In section III we develop the expected cross-correlation of the interferometer samples in terms of the receiving filter transfer functions and the sampling clock parameters, and we review features of the delay estimation process which admit systematic errors. Supporting transform analysis for this development appears in Appendix A. The sensitivity of the VLBI time delay to filter variations is estimated in section IV. The principal result of this section is that quite plausible variations in these filters can result in changes in the VLBI time delay of 5-15 cm. In section V, the last section of this article, we estimate the error potential inherent in the necessary receiver channel modeling for bandwidth synthesis data. A phase calibrator which is itself

assumed perfect is used in some parts of this analysis. The principal result of this section is that errors due to channel modeling, which can be on the order of 0.5 to 1 m without calibration, can be held to generally below 1 cm if two tones from a "perfect" phase calibrator are placed in each of the synthesis channels. Evaluation of a real phase calibrator is another subject.

## II. The VLBI Receiving-Processing System

Figure 1 shows the portion of the VLBI system which is of concern here. The radio-source and transmission path, while shown, are not explicitly of concern, and are included as a reference platform for the behavior of the system. The radio source is assumed to be a point source, and the transmission path nondispersive.

The radio source emits a low-level white noise process which travels by separate paths to receiving stations. The transmission path delays, '$d_1$' and '$d_2$', are time-varying, in general, as are the oscillator reference phases, '$\phi_1$' and '$\phi_2$', and the delays into the samplers, '$q_1$', and '$q_2$'. The station frequency and time references provide a coordinate system for the description of the received signals. The delays to the stations are specified as "backward-looking," with respect to their time of arrival at the receiving stations. As expressed in general coordinate time,

$$e_1'(t) = e[t - d_1(t)]$$

$$e_2'(t) = e[t - d_2(t)]$$

(1)

The reconciliation between this general coordinate time and the two station time-coordinates is a part of the job of the parameter estimator.

Each receiving system adds its own (independent) white gaussian noise process, of temperature approximately 20 K at the maser amplifier. The maser amplifier contains the filter $H_i(s)$, with a variable gain and bandwidth. A plausible model for the maser-amplifier when operating in wideband mode is a double-tuned filter plus a transmission line. The total maser delay is ~16 m (Ref. 2).

The output of each maser amplifier, still at microwave frequencies, is mixed with a local-oscillator before subsequent filtering by $G_i(s)$ and sampling. The filters $G_i(s)$ are assumed to be at least zonal-low-pass, so that second-harmonics are rejected. The mixer itself has a noise temperature of several

thousand K, which is negligible as long as we are near the high-gain region of $H_i(s)$.

For wideband-sampling (WBS), the filters $G_i(s)$ represent the (50-MHz) IF filters of the Block III or Block IV Receivers. For bandwidth-synthesis (BWS) processing (Ref. 3), the $G_i(s)$ represent the final narrow-band channel filters, while the pertinent portions of the IF filters are absorbed into the RF filters $H_i(s)$. When needed, we will include other details of the physical system, such as the implicit filtering of the quadrature SSB demodulator into the two-filter model shown by appropriate interpretation of the $H_i(s)$, $G_i(s)$ parameters.

The sampling of the data at the output of the filters $G_i(s)$ establishes a firm and manipulable coordinate system within which the subsequent cross-correlation and processing are performed. Proper interpretation of the correlation products requires a precise understanding of the continuous and time-varying time coordinates within which the receiver filters and the problem geometry are separately defined. Jitter of the sampling operation per se and pseudorandom transport lags of the receiving system are included within quantizer delays $q_i(t_i)$. The correspondence between station times $t_1$, $t_2$, which establishes the coordinate base for the data processing, and the general coordinate time within which the problem geometry is intrinsically defined, will be established by a redefinition of the geometric time delays.

## III. Correlation and Estimation for VLBI DATA

In this section we derive the cross-correlation to be observed between the two sampled data streams as a function of the physical filters which precede the sampling.

At the sampler, the station clock which controls the sampling places an absolute and incorruptible time base into the data. Except for phase noise, this same time base is also coherent with the local oscillator and any calibration system which may be used. It is convenient, furthermore, to consider the filters at a given station as defined within the time reference system of that station's clock. This is consistent with our belief that the best knowledge of the filter characteristics at a station will come through measurements during or in conjunction with a VLBI experiment. Such measurements will of necessity specify these filter characteristics with respect to the station time-base.

Let the input to the receiver's low-noise-amplifier be specified as $a_1(t_1)$ within the reference frame of the station 1

clock. The input to the station 1 sampler $c_1(t_1)$ can be written by inspection as

$$c_1(t_1) = \int_{-\infty}^{t_1 - q_1(t_1)} g_1[t_1 - q_1(t_1) - \eta_1]$$

$$\left\{ \cos[\omega_1 \eta_1 + \phi_1(\eta_1)] \int_{-\infty}^{\eta_1} h(\eta_1 - \xi_1) a_1(\xi_1) d\xi_1 \right\} d\eta_1$$

$$(2)$$

where $g_1(x)$, $h_1(x)$ are the impulse responses of the filters $G_1(s)$, $H_1(s)$, and $q_1(t_1)$, and $\phi_1(\eta_1)$ are the sampler input delay and the local-oscillator phase, respectively.

To develop $c_1(t_1)$ further, in terms of the radio-source emissions, and permit the calculation of the cross correlation, $a_1(t_1)$ needs to be expressed in terms of $e(t)$ and $d_1(t)$, both of which are known as functions of general coordinate time, and not as functions of station time. Let the function $\Delta u_1(t_1)$ represent the correction term: Station 1 clock-time minus general coordinate time; i.e., if

$$t_1 \text{ is Station 1 clock time}$$

then $\hspace{5cm}$ (3)

$$t = t_1 - \Delta u_1(t_1)$$

is the corresponding general coordinate time.

In general coordinate time $t$, the radio-source signal at the station 1 antenna $e_1'(t)$ is

$$e_1'(t) = e[t - d_1(t)] \hspace{2cm} (4)$$

where $e(t)$ is the radio source emission at time $t$, and $d_1(t)$ is the backward looking time delay of the path to station 1 from radio source.

Let us define a clock-adjusted delay function $k_1(t_1)$ to be

$$k_1(t_1) = \Delta u_1(t_1) + d_1[t_1 - \Delta u_1(t_1)] \hspace{1cm} (5)$$

As both $d_1(t)$ and $\Delta u_1(t_1)$ are slowly varying functions, so too is $k_1(t_1)$. The input to the Station 1 receiver is then expressed in Station 1 clock time as

$$a_1(t_1) = e[t_1 - k_1(t_1)] + n_1(t_1) \hspace{1cm} (6)$$

A completely parallel notation applies to the signals at Station 2.

Let us expand $k_1(\xi_1)$ in the neighborhood of $t_1$, such that

$$k_1(\xi_1) = k_1(t_1) + \sum_{l=1}^{\infty} k_{1l}(t_1) \cdot (\xi_1 - t_1)^l \hspace{1cm} (7)$$

From physical considerations, we expect that $|k_{11}(t_1)|$ will be less than $10^{-5}$, $|k_{12}(t_1)|$ less than $10^{-11}$, and subsequent terms correspondingly smaller. We note further that the filters $G_1(s_1)$, $H_1(s_1)$ are relatively wideband and thus have short memory. Let $g_1 \odot h_1(t_1 - \xi_1)$ denote the combined impulse response of these filters as in Eq. (2). We expect the magnitude of $g_1 \odot h_1(t_1 - \xi_1)$ to be such that the contribution to $c_1(t_1)$ from $a_1(\xi_1)$ is negligible (e.g., below $10^{-10}$ of the total) for all $\xi_1$ such that $|t_1 - \xi_1| > 10^{-4}$. From the anticipated magnitude of the $k_{1i}(t_1)$ terms in Eq. (7), the error in estimating $k_1(\xi_1)$ by a linear approximation in the neighborhood of $t_1$, i.e., $|k_1(\xi_1) - k_1(t_1) - k_{11}(t_1) \cdot (\xi_1 - t_1)|$, is negligible (e.g., below $10^{-18}$) for all $|t_1 - \xi_1| < 10^{-4}$. Thus, we have:

$$k_1(\xi_1) \approx k_1(t_1) + k_{11}(t_1) \cdot (\xi_1 - t_1) \hspace{1cm} (8)$$

as a valid approximation to $k_1(\xi_1)$ for use in evaluating the needed cross-correlations via Eqs. (2) and (6). The precise level of accuracy of this approximation is a function of the specific filters (and processing) used, and can be evaluated later, if desired. The validity of this approximation within the context specified permits the use of transform-domain techniques for performing the convolutions in Eq. (2). For notational convenience, we will define new constants $p_1$, and $p_{11}$, which are implicitly functions of $t_1$, and reinstate the explicit dependence when necessary. Define

$$p_1 = k_1(t_1) - k_{11}(t_1) \cdot t_1$$

$$p_{11} = k_{11}(t_1)$$

so

$$k_1(\xi_1) \approx p_1 + p_{11} \cdot \xi_1 \hspace{1cm} (9)$$

in the neighborhood of $t_1$.

We also need to assume that $q_1(t_1)$ and $\phi_1(\eta_1)$ are slowly varying, and that $\phi_1(\eta_1)$ is well approximated by $\phi_1(t_1)$ within the context of the convolutions in Eq. (2). The

corresponding definitions and assumptions apply to Station 2 filters and data.

Within this context, the input to the Station $i$ receiver is

$$a_i(t_i) = e(t_i - p_i - p_{i1}t_i) + n_i(t_i) \qquad (10)$$

and the input to the Station $i$ sampler-limiter is

$$c_i(t_i) = \int_{-\infty}^{t_i - q_i} g_i(t_i - q_i - \eta_i) \left[ \cos(\omega_i \eta_i + \phi_i) \right.$$

$$\int_{-\infty}^{\eta_1} h_i(\eta_i - \xi_i)$$

$$\left. \cdot [e(\xi_i - p_i - p_{i1}\xi_i) + n_i(\xi_i)] \, d\xi_i \right] d\eta_i \qquad (11)$$

where we have suppressed the explicit dependence upon $t_1$ and $t_2$ for the functions $q_i$, $\phi_i$, as well as for $p_i$, $p_{i1}$, as declared earlier.

The processing of VLBI data is performed upon a sampled hard-limited version of the signals $c_i(t_i)$. The cross-products of data samples from the two stations exist only at discrete and regularly spaced values of $t_1$ and $t_2$. Calculation of the expected value of these cross-products from the foregoing definitions is straightforward but tedious, and is performed in Appendix A. Denote this expected value as $S'_L(\tau_3, \phi_3 : t_1, t_2)$ when written in terms of the two station clock-time indices. For weak signals, the typical case, we have from the appendix that

$$S'_L(\tau_3, \phi_3 : t_1, t_2) \simeq \frac{2}{\pi} \frac{S'_c(\tau_3, \phi_3 : t_1, t_2)}{\sqrt{A_{c1}(0,0) \cdot A_{c2}(0,0)}} \qquad (12)$$

where $S'_c(\ldots)$ is the cross-correlation for nonlimited samples, $A_{ci}(\ldots)$ are the $i^{\text{th}}$ receiver autocorrelations, and with some manipulation,

$$\tau_3 = \frac{t_2 - t_1 - k_2 + k_1}{1 - k_{21}} + q_1 \cdot \frac{1 - k_{11}}{1 - k_{21}} - q_2 \qquad (13)$$

$$\phi_3 = \omega_2 \cdot t_2 + \phi_2 - \omega_1 \cdot t_1 - \phi_1 - \omega_2 \left( \frac{t_2 - t_1 - k_2 + k_1}{1 - k_{21}} \right)$$

$$- q_1 \left( \omega_2 \frac{1 - k_{11}}{1 - k_{21}} - \omega_1 \right)$$

$$S'_c(\tau_3, \phi_3 : t_1, t_2) = \frac{N_e}{8} \cdot \frac{1}{1 - k_{21}} \int_{-j\infty}^{+j\infty} \frac{d\eta}{2\pi j} e^{-\eta \tau_3} G_2(-\eta)$$

$$\cdot \left\{ e^{-j\phi_3} H_2(-\eta + j\omega_2) \right.$$

$$\cdot H_1 \left[ (\eta - j\omega_2) \frac{1 - k_{11}}{1 - k_{21}} \right]$$

$$\cdot G_1 \left[ (\eta - j\omega_2) \frac{1 - k_{11}}{1 - k_{21}} + j\omega_1 \right]$$

$$+ e^{+j\phi_3} H_2(-\eta - j\omega_2)$$

$$\cdot H_1 \left[ (\eta + j\omega_2) \frac{1 - k_{11}}{1 - k_{21}} \right]$$

$$\left. \cdot G_1 \left[ (\eta + j\omega_2) \frac{1 - k_{11}}{1 - k_{21}} - j\omega_1 \right] \right\}$$

$$A_{ci}(0,0) = \frac{N_i + N_e}{8} \int_{-j\infty}^{+j\infty} \frac{d\eta}{2\pi j}$$

$$\left[ G_i(-\eta) H_i(-\eta + j\omega_i) H_i(\eta - j\omega_i) G_i(\eta) \right.$$

$$\left. + G_i(-\eta) H_i(-\eta - j\omega_i) H_i(\eta + j\omega_i) G_i(\eta) \right]$$

The difference in the clock-adjusted delay terms, $k_1(t_1) - k_2(t_2)$, is a combination of a diurnal sinusoid plus fixed and linear offsets and other effects due to the propagation medium. Over any single VLBI observation, it can usually be assumed that this clock-adjusted differential delay is known a priori except for an unknown fixed and (small) linear offset which must be solved for in order to characterize the observation. The correlation amplitude, or the radio source noise density $N_e$, is also an unknown to be determined. The receiving instrument itself can add two more unknown parameters to the set which must be solved for, namely, the local oscillator differential phase and phase-rate relative to the

57

station standards. As can be deduced from Eq. (13), the differential delay induces a phase effect which is indistinguishable from the instrument-induced phase effect. Thus, to characterize any one VLBI observation, there are five parameters: correlation amplitude, delay, delay-rate, phase, and phase-rate, which are unknowns to be solved for. In principle, these five parameters could be extracted directly from the bit-wise cross products, although in practice pre-sums (Ref. 4) are generated to reduce the amount of computing that must be done. For the purposes of this present section, we will assume that this intermediate step is non-lossy, and produces a result identical to that which would be obtained directly from the bit-wise cross products.

To a communications-oriented engineer, the "obvious" technique for estimating the parameters of interest is that of maximum-likelihood, or a numerically tractable approximation to it. To others, the method of minimum mean-square error (MSE) fit seems proper. In either case, an assumed model for the receiver's filter structure is an important part of the estimation procedure. Mismatch between this model and the actual cross-correlation appears to be the sole source for biases in the estimates. The minimum MSE, or least-squares estimation procedure is at least an approximation to maximum likelihood that should produce estimates which are "close" in some sense. In particular, we note that the linear term of the Barankin (Ref. 5) lower bound to the RMS deviation of a parameter estimated via maximum likelihood for a process embedded in Gaussian noise is identical to the formal standard deviation for that same parameter when estimated by the method of least squares.

The linear least-squares procedure is defined as follows (Ref. 6): Let x be an m-vector of parameters, $A$ a $k$-by-$m$-matrix of coefficients, 'n' a $k$-vector of noise perturbations, and y a $k$-vector of observations, such that:

$$\mathbf{y} = A \cdot \mathbf{x} + \mathbf{n} \qquad (14)$$

Assume that n has zero mean with covariance matrix

$$V = \left\langle \mathbf{n} \cdot \mathbf{n}^T \right\rangle \qquad (15)$$

where $\left\langle \cdot\cdot \right\rangle$ denotes expected value, and $T$ denotes transpose. Then the least-squares solution for x, $\widehat{\mathbf{X}}$ is given by

$$\widehat{\mathbf{X}} = (A^T V^{-1} A)^{-1} A^T V^{-1} \mathbf{y} \qquad (16)$$

which has formal error covariance on **X** given by

$$\left\langle \widehat{\mathbf{X}}_e \cdot \widehat{\mathbf{X}}_e^T \right\rangle = (A^T V^{-1} A)^{-1} \qquad (17)$$

when

$$\widehat{\mathbf{X}}_e = \widehat{\mathbf{X}} - \left\langle \widehat{\mathbf{X}} \right\rangle$$

A non-linear problem such as that posed by parameterizing Eq. (13) may be solved by assuming that it is incrementally linear in the neighborhood of some approximate solution and then solving an iterative series of (hopefully converging) linear least-squares problems. If such linearization is valid at the final solution point, and if the norm of the formal error covariance Eq. (17) is small, then the formal error covariance of the linearized problem is also the formal error covariance of the nonlinear base problem. The A-matrix is to be interpreted as the matrix of partial derivatives of the $k$ observation values with respect to the $m$ parameters.

The $l + 1^{\text{st}}$ step of this iterative procedure is given by

$$\widehat{\mathbf{X}}_{l+1} = \widehat{\mathbf{X}}_l + (A_l^T V^{-1} A_l)^{-1} A_l^T V^{-1} \left[\mathbf{y} - \widehat{\mathbf{Y}}(\widehat{\mathbf{X}}_l)\right] \qquad (18)$$

where the subscript on $A_l$ indicates that the partial derivatives which comprise this matrix are evaluated at $\widehat{\mathbf{X}}_l$, the prior best estimate of the parameters **X**. $\widehat{\mathbf{Y}}(\widehat{\mathbf{X}}_l)$ is the modeled expected value of the observable $y$, evaluated at the parameter point $\widehat{\mathbf{X}}_l$. Convergence is indicated when no significant change occurs in $\widehat{\mathbf{X}}_{l+1}$. This will occur at the "true $X$" if the functional dependence of $\widehat{\mathbf{Y}}(\mathbf{X})$ upon **X** is correctly specified, but may occur almost anywhere else if our model is wrong.

This feature of the processing implies that there is in fact *no* bias built into the system until the estimation of parameters. Even phenomena as apparently insidious as multipath are but linear filtering operations which can be modeled and their effect eliminated as long as this effect is not so severe as to destroy the 1:1 mapping of input to output. They may cause severe degradations, but not bias errors, if properly modeled.

In later sections, when we attempt to evaluate the biases which result either from our lack of knowledge about the system, or laziness in developing the model used to estimate parameters, we will assume that such biases are small, within the linear range of the final iteration step Eq. (18). With this assumption, we can compute the bias for a model mismatch directly from Eq. (18) by replacing the observed y with a correct model for $\mathbf{Y}(\widehat{\mathbf{X}}_l)$. Furthermore, if the bias is not large, we could equally well approximate the bias for some "pro-

posed model" if we knew what the "correct model" was and solved Eq. (18) using the "proposed model" as the observed vector $y$ and the "correct model" as the model for functional dependence. This latter form is more convenient for reviewing a wide variety of proposed models, and will be used in the following sections.

## IV. Sensitivity to Receiver Filter Variations

As noted earlier, bias errors in the estimation of the VLBI cross-correlation parameters arise predominantly from mismatch between the model for the receiver filter structure and the receiver itself. For this section, we will assume that we know exactly the *form* of the receiver filters, but know the filter parameters with some small error. This error could arise from variations in filter component values during manufacture, from errors in measurement of the parameters, or from environmental effects (predominantly thermal) during operation of the system. Such error is of particular interest when we are *not* using real-time calibration. If properly done, calibration should remove most of the variation observed.

For specificity, we will assume that the maser front-end amplifier and mixer-amplifier $H_i(s)$ correspond to three pole-pair filter functions which were observed in a VLBI experiment (Ref. 7). For bandwidth synthesis operation, the final-filters $G_i(s)$ correspond to 7-pole Butterworth filters with 2-MHz passbands (Ref. 8). Filter functions for the quad-hybrids which implement a physical single sideband (SSB) demodulator are assumed to be very simple 4-pole networks covering 0.1 to 2 MHz (e.g., Ref. 9).

Variations in the discrete component filters can be reasonably anticipated to be on the order of one part in $10^3$ due to environmental changes. Variations in manufacture could be more than one part in $10^2$ unless special care is taken in selecting components. The low-noise maser amplifier is considerably more stable than this, but is subject to manual tuning, so variations between experiments could be on the order of a few parts in $10^3$. Within any one experiment, laboratory evidence (Ref. 2) suggests that variations can be held to one part in $10^5$ or $10^6$. But recent field tests in preparation for the Pioneer Venus atmosphere wind experiment (Ref. 10) observed narrow-band group-delay variations on the order of a nanosecond, which corresponds to filter-parameter changes of a part in $10^4$, far in excess of the laboratory experience.

For the numerical results to be presented, the offset in correlation parameters is calculated using Eq. (18) for errors in filter pole positions of one part in $10^4$. For the results to be

presented, the pre-whitening filter $V^{-1}$ is ignored and treated as an identity matrix. Poles are adjusted one at a time with the exception that complex pole pairs are moved pair-wise, with their real and imaginary parts varying individually, as befits actual physical parameter variations. Variations of this magnitude appear to be within the linear range of the MMSE parameter-estimator so that parameter biases for the anticipated physical variations can be taken directly from these calculations. The anticipated overall delay variation will be interpreted to be the root-sum-square (RSS) of the effects of varying the individual filter parameters, since the parameters will all move under the environmental forces, but not coherently.

Our interest for this section is exclusively on the effects of filter changes, so we must avoid errors in calculation due to "end-effects" from the finite-length data record. This can be done directly by working with a data record which is long enough so that whatever end-effects may exist are reduced to a negligible level relative to the complete "traces" of the cross-correlation function which occur through the middle of the record. We can also approximate this long-record processing by utilizing precisely one trace of the cross-correlation function covering a delay-distance equal to the number of lags to be used in normal processing. Since this "trace-mode" is computationally much cheaper, it will be used in the majority of our calculations, and the results verified by a few calculations with long records.

Figure 2 (from Ref. 7) shows the assumed passbands for the maser front-end amplifier and mixer amplifier. Each receiver exhibits three distinct complex pole-pairs, two of which are probably in the maser-amplifier itself, and the third in the succeeding electronics. The effect of filter pole motion on parameters estimated for the cross-correlation of these two passbands was calculated for full-band sampling using an 8-lag cross-correlation trace at doppler of $1 \times 10^{-5}$. Table 1 gives the offset in delay and phase caused by changes of one part in $10^4$ of the imaginary parts of the filter pole-pairs. Offsets caused by the real-parts of these filter pole-pairs were observed to be typically 2 orders of magnitude smaller than those caused by the corresponding imaginary part, and thus were not included in Table 1. Identical results were obtained at $1 \times 10^{-7}$ doppler. This example was also calculated for a record length of 5 sec at $1 \times 10^{-5}$ doppler, with a resultant RSS time delay offset of 0.22 ns, reasonably close to the 0.23 ns found by the single-trace calculation. If, as discussed above, we can anticipate variation in the maser-amplifier of one part in $10^4$, we should anticipate a related time-delay estimate offset of about 0.23 ns, or 7 cm, equivalent path-length, which is variable and dependent upon environmental factors.

Bandwidth synthesis operation considerably complicates the task of understanding the receiver parameter effects. Segments of the RF passband are extracted by a single sideband (SSB) demodulator with an appropriately set local oscillator and low-pass filter. We consider only the two most widely separated segments for which the synthesized time-delay estimate is the ratio of the difference of phases (of two selected segments) to the difference of center frequencies (of these two segments). The individual channel group delay is now only an auxiliary parameter. The effect of filter pole motion on parameters estimated for the cross-correlation of segments of the RF passbands was calculated at $10^{-7}$ doppler using a single trace of the cross-correlation function for local-oscillator (LO) frequencies ranging from 2250 to 2315 MHz. Results for frequencies outside of the passbands (2265 to 2300 MHz) in Fig. 2 are questionable because the noise from the mixer-amplifier (3000 K) is becoming significant with decreased gain and is not included in the calculations.

Variations in the final filter of the BWS demodulator (a 7-pole Butterworth at 2 MHz) must be considered in two forms, depending upon whether a single filter is used and time-multiplexed between segments of the passband, or different filters are used in each segment. In either case, the resultant effect is quite small, so a typical example will be discussed instead of a range of results. For a *common* filter, operating with LO's of 2260 and 2300 MHz, the RSS of differenced phase offsets for the 14 poles in these filters is approximately $3.6 \times 10^{-3}$ rn, which indicates that a synthesized delay offset of only 15 picoseconds should be expected for component variations of one part in $10^2$ (Table 2). If *different* filters are used with LO's of 2260 and 2300 MHz, the RSS of the phase offsets for the 28 poles of these filters is approximately $28 \times 10^{-3}$ rn, which indicates that a synthesized delay offset of 0.11 nanoseconds (3.3 cm) should be anticipated for component variations of one part in $10^2$. Assuming that manufacturing-related tolerances on the order of one part in $10^2$ are uncompensated and uncalibrated, configuration-dependent offsets in the synthesized delay (2260-2300) of 3-5 cm can be anticipated. As environmental changes to the filters should be on the order of a part in $10^3$, changes in the synthesized delay should be less than 1 cm.

Variations in the quad-hybrid demodulator filters also affect results differently, depending upon whether a single demodulator is time-multiplexed between channels, or multiple demodulators are used. Our calculations were performed using very simple 4-pole quad-hybrids covering 0.1 to 2 MHz. Since *real* quad-hybrids may have 12 or more poles (and zeros), the offsets due to their variations are likely to be twice what is observed numerically here. For a *common* demodulator, operating with LO's of 2260 and 2300 MHz, the RSS of differenced phase offsets for the 8 poles in these demodulator filters is approximately $0.43 \times 10^{-3}$ rn, which indicates that a synthesized delay offset of less than 2 picoseconds can result from component variations of one part in $10^2$ (Table 3). If *different* demodulators are used with LO's of 2260 and 2300 MHz, the RSS of the phase offsets for the 16 poles of these .filters is approximately $5.7 \times 10^{-3}$ rn, which indicates that a synthesized delay offset of about 23 picoseconds (0.7 cm) can result from component variations of one part in $10^2$. Assuming that manufacturing-related tolerances on the order of one part in $10^2$ are uncompensated and uncalibrated, configuration-dependent offsets in the synthesized delay (2260-2300) of about 1 cm can be anticipated. Environmental changes to the demodulator synthesized delay should be on the order of 1 mm. Even if a realistic quad-hybrid, because of its increased complexity, has variations of twice that of the simple one used here, the offsets due to the quad-hybrid parameters are still small (in an RSS-sense) compared to the offsets due to the final filter parameters. This may, however, be an overly simplistic view, as it ignores the active electronic elements which interconnect the two filters in the quad-hybrid to make up the demodulator proper. Testing of a complete demodulator unit appears to be the best way to ensure a realistic understanding of demodulator variations.

The effects of the maser-front-end amplifier variations are always common between segments of the passband, and so are relatively independent of whether a single time-multiplexed demodulator and final filter or multiple ones are used. The actual effects of these variations do depend significantly upon the placement of the selected channel within the passband. Figure 3 shows the channel group delay offset caused by a change of one part in $10^4$ in the imaginary parts of each of the 6 RF poles as a function of the LO frequency. The maximum offset is on the order of 1 nanosecond, which is approximately that observed in field experiments (Ref. 10), and lends credence to the belief that anticipated physical variations should be on the order of one part in $10^4$. Figure 4 shows the channel phase offset caused by a change of one part in $10^4$ in the imaginary parts of each of the 6 RF poles as a function of the LO frequency. The data in Fig. 4 can also be presented as in Fig. 5 which shows the RSS synthesized delay offset resulting from filter pole variation of one part in $10^4$ with various selected spanned bandwidths, as indicated.

If we can anticipate variation in the maser-amplifier of one part in $10^4$, we should anticipate a related synthesized time-delay estimate offset between 0.2 and 0.5 ns. (6 to 15 cm path length), which is variable and dependent upon environmental factors. The offset observed is a function of the placement of the selected channel within the passband, and it appears that we are at least as likely as not in doing BWS to select channels for which the sensitivity is 20 to 50% larger than the sensitivity of the full band sampling. We note,

however, from Fig. 4 that the phase sensitivity decreases *outside* of the main passband, so that *if*, for example, we could successfully operate at 2255-2315, the sensitivity appears to be only 0.034 ns for filter variations of one part in $10^4$. These results are related to the physical model assumed for TWM variations, and should be verified experimentally.

We need also to be aware that we never really know the receiving filters, as has been assumed in this section, but are forced to estimate it through measurements and/or calibration. The effect of channel estimation and calibration is the subject of the next two sections.

# V. Channel Modeling for Bandwidth Synthesis

The intent of this section is to determine the minimum complexity receiver models for the bandwidth synthesis VLBI receiver which will yield suitably small errors in the resultant estimates. We will, in the following, propose and evaluate channel models of varying complexity. The results of this section should *not* be construed as representing the performance of any existing VLBI processing, although the tools employed here can be applied to any existing or proposed processing schemes.

The receiver passbands of Fig. 2 are again assumed to be the RF-front-end filter. There is reason to believe that these receivers represent a somewhat pathological choice, because the mismatch between passbands, while an example of a real experiment, is nevertheless a worse condition than should be achieved in a "typical" experiment with careful tuning of the traveling-wave masers (TWM). Therefore, we believe that if a channel modeling scheme can be made to give some specific level of accuracy with this example-pair of receiver passbands, then this same level of accuracy should be achievable in practice in most experiments.

The BWS final filter will be assumed to be a 2-MHz-wide 7-pole Butterworth, which is itself a practical approximation to an ideal *square* passband. The assumed SSB demodulator is the simple 4-pole R-C type used in Section IV.

The most naive channel model we are tempted to try is the mathematical square passband, both with and without calibration. Calibration consists of a very stable and well-controlled pulse train which is injected into the signal path ahead of the maser (Ref. 11). In the frequency domain, this pulse train is seen as a "comb" of pilot-tones with related phases, of which at least one, or perhaps many may appear in each of the BWS channels. If one tone appears in each channel, it is capable of measuring (relative to itself) the phase of the local oscillator

and approximating the phase-effect of the receiving filters. A second tone gives some information about the transport lag in the receiving system. It also gives some information about the relative amplitude of the receiving filters. Increasing the number of tones in each channel improves the ability to measure the transfer function of the receiver filters (Ref. 12). We assume, for now, that the calibrator itself is "perfect."

The models for which the bias offsets were calculated are of two general types: "Type A" models incorporate a mathematically square 2-MHz passband with zero, one, or two pilot tones; "Type B" models incorporate the transfer function of a Butterworth filter and quad-hybrid demodulator, which is nominally the same as that in the assumed receiver function, along with zero, one, or two pilot tones. All demodulators select upper sideband. Where one pilot tone is used, it is placed 0.5 MHz from the lower band-edge. Where two pilot tones are used, they are placed 0.5 MHz from each band-edge. Models A1 and B1 utilize no pilot tones, but their calculation assumes that the phase of the LO is stable and known, so that the only unknown phase is that induced by the receiving filters. Models A2 and B2 utilize one pilot tone to calibrate the phase shift through the unknown receiver filters, and along with that, the phase of the LO. Models A3 and B3 utilize two pilot tones to jointly calibrate the phase shift and transport-lag equivalent of the unknown receiver filters. Model B4 utilizes the relative *magnitudes* of the filter responses to the two pilot tones to estimate the parameters of single-tuned-filter approximation to the RF filter $H(s)$. The residual phases of these pilot tones are then used to determine the phase-shift and transport-lag of the receiver, as in Model B3.

As a practical matter, when two pilot tones are used in each channel, their frequencies would be slightly displaced from the multiples of 0.5 MHz in order to avoid harmonic interaction.

The Model B4 transfer function is of the form

$$B4H(s) = \frac{A \cdot s \cdot e^{\tau s + j\phi}}{(s - y - jx)(s - y + jx)} \qquad (19)$$

where the *five* parameters: $A$, $\tau$, $\phi$, $y$, and $x$ are to be chosen to best fit the amplitude and phase at each of two pilot tone frequencies. Since there is one more unknown than measurement, we complete the problem definition by assuming that the bandwidth $y$ is as large as possible consistent with Eq. (19), but not larger than some preset value $y_0$. We have taken $y_0 = 40$ Mrn/sec to correspond roughly to the individual poles in Fig. 2. The approximate solution for the parameters $x$ and $y$ is as follows: Let $w_1$ and $w_2$ be the (angular) pilot tone frequencies, and let $\Delta = w_2 - w_1$. Let $H1$, and $H2$ be the measured complex response of the receiver passband at $w_1$ and

$w_2$, exclusive of the final filter and demodulator. Let the preliminary values for $x$ and $y$ be $x_0 = (w_1 + w_2)/2$ and $y_0$ as above. Then we take

$$\rho = \left| \frac{H_1}{H_2} \right| \cdot \frac{w_2}{w_1} \cdot \sqrt{\frac{y_0^2 + (w_1 + x_0)^2}{y_0^2 + (x_0 + w_2)^2}}$$

$$y = \min \{y_0, \Delta \cdot \rho/(\rho^2 - 1)\} \qquad (20)$$

$$x = w_1 + \frac{-\Delta + \sqrt{\rho^2 \Delta^2 - y^2 (\rho^2 - 1)^2}}{(\rho^2 - 1)}$$

to be our approximate solution to the magnitude part of Eq. (19). The phase and delay parameters are determined after inserting these $x$ and $y$ values into Eq. (19).

The offset between the parameter estimates for these models and the assumed true receiver has been calculated using a single trace of the cross-correlation function — usually covering six lags. The phase is in all cases referenced to the frequency at the passband center as determined from the assumed receiver's transfer function, and not from the pilot-tone responses. In practice, this reference frequency would be determined from the autocorrelation of the recorded data.

Figure 6 shows the estimated differential phase offset for all models at a doppler of $1_{10}{-}7$ as a function of mixing frequency. With no pilot tones, the offset phase swings by nearly 1 radian as the mixing frequency traverses the frequencies below 2270 MHz, where the two RF passbands show significant missmatch. Were we to do delay synthesis using 2265-2305, a delay error of about 0.5 meter would result. A single pilot tone is seen to be sufficient to reduce this swing to about 0.1 rn, and the synthesized delay error to less than about 10 cm. The use of transport-lag information from the second pilot tone reduces the phase swing still further to below 0.02 rn. And at this scale, model B4 appears perfect.

At an expanded scale, Figure 7 shows the offset phase as a function of mixing frequency for models 2-4 at a doppler of $1_{10}{-}7$. An identical figure would be drawn for any doppler smaller than $1_{10}{-}7$. Increasing doppler, however, does change the offset phase as can be seen by observing Figures 8, 9, and 10 which represent dopplers of $1_{10}{-}6$, $3_{10}{-}6$, and $1_{10}{-}5$, respectively. The largest differential doppler to be expected for two Earth-bound receivers is on the order of $3_{10}{-}6$. At this doppler, *all* models have shown some phase shift relative

to $1_{10}{-}7$ doppler, and the Type-A models show phase shift approaching 0.03 rn. The effect of doppler on synthesized delay is not as large as on channel phase because the phase shift is in the same direction in channels at all frequencies. Figure 11 shows the synthesized delay offset for mixing frequencies 2260-2300 as a function of applied doppler. Model B4 changes by only 0.01 ns (0.3 cm) for doppler changing $1_{10}{-}7$ to $1_{10}{-}5$. Model B3 changes by 0.05 ns (1.5 cm) and models B2, A2, and A3 changes by 0.06 ns (1.8 cm) for doppler increasing from $1_{10}{-}7$ to $1_{10}{-}5$. For real dopplers restricted to below $3_{10}{-}6$, the synthesized delay change is negligible for model B4, and below 0.02 ns (0.6 cm) for models 2 and 3. The part of the synthesized delay offset which does not depend on doppler is approximately 0.4 ns for the No. 2 models, 0.05 ns for the No. 3 models, and apparently negligible for model B4.

The "end-effects" from finiteness of the data record can be greatly enhanced by considering parameter estimation for a single-trace of the cross-correlation function which has been asymmetrically truncated. Even with this exaggeration, model B4 exhibits less than 1 cm synthesized delay offset (2260-2300) when receiver and model final filters are perfectly matched. For the more normal mode, sample calculations with a record length of 15 sec and $10^{-7}$ doppler have exhibited no end-effect variations with any model larger than 1 mm in synthesized delay for perfectly matched receiver and model final filters. End-effects should be reexamined with mismatched final filters.

In the foregoing, Type-B models have been generated assuming that the transfer functions of the demodulator and final filter are exactly known. At best, these filters are subject to manufacturing tolerances, and at worst, the quad-hybrid may be some company's trade secret, and its transfer function known to us only through our measurements. The exploration of this space is similar to that of Section IV, but is compounded by carrying several alternative models here. Some exploration has been done which should approximate worst-case for the demodulation filters. Figures 12 and 13 show the estimated channel phase which results when the demodulator transfer function of Station 1 only is scaled upward in frequency by 10%, for dopplers of $1_{10}{-}7$ and $1_{10}{-}5$. The shift to the No. 2 models' phase is on the order of 0.01 rn and varies with doppler and mixing frequency. The shift to the phase of model B4, or No. 3, is of the order of 0.003 rn, and is again dependent upon doppler and mixing frequency. Thus an unlikely large error in our knowledge of the demodulator filters results in a synthesized delay error which is at worst 1-2 cm for any of the pilot-tone models. If we try at all while the equipment is being built, we should be able to know these filters to within a few percent, and hence reduce errors related

to modeling of this portion of the equipment to less than 0.5 cm in synthesized delay.

Errors in generating and/or measuring the phase calibrator tones cause channel phase errors in the relatively obvious way. Phase errors of $10^{-2}$ rn on a calibration tone induce channel phase errors of 0.5 to $2 \times 10^{-2}$ rn. Amplitude errors of 1% on a calibration tone induce channel phase errors of roughly $10^{-3}$ rn in model B4, with no effect on the other models. There is thus a need to hold at least the differential phase errors between the calibration tones in the upper and lower bandwidth synthesis channels to well below $10^{-2}$ rn if accuracies on the order of 1 cm are to be achieved with 40-MHz spanned bandwidth. This requires careful design and fabrication of the calibrator itself, and SNR's of at least 50-60 dB on the detected calibration tones.

Assuming that a suitable calibrator can be achieved, we summarize the results of this section as follows: If no calibration is used, the receiver filters alone can represent as much as a 1-meter offset in direct delay if the phases of the mixing references are known. A single calibration tone in each channel can reduce this offset to perhaps 10-15 cm, of which only a few cm is doppler-dependent. Using two calibration tones in each channel together with modeling technique B4 can further reduce this offset to under 1 cm. This last result depends upon our knowing the final filter and demodulator filters to within a few percent, and deserves to be reevaluated using the actual transfer functions of a physical device, instead of the "publication" filters employed here.

## VI. Discussion and Summary

Perhaps the greatest difficulty in obtaining definitive results for the biases induced by the VLBI instruments is the wide range of possible configurations and parameter values which can characterize the instrument. In such a situation, the seemingly only way to get numerical results is to assume an example system which is a reasonable approximation to reality and evaluate its characteristics in detail. To the extent that our example approximates some real system, our numerical results can then be used with some care to estimate the behavior of that system. Our software tools may be useful for evaluating systems which are not close to the examples developed here.

We evaluated the sensitivity of the VLBI estimated time delay to plausible variations in the receiver filter parameters. Shifts on the order of one part in $10^4$ of the RF filter poles induce delay errors of roughly 7 cm with full band sampling, and between 6 and 15 cm with bandwidth synthesis. Shifts in the 2-MHz channel filters used for bandwidth synthesis were less deleterious than had been expected. Environmentally caused shifts on the order of one part in $10^3$ of the channel filter poles induce delay errors of less than 1 cm. However, if separate channel filters are used, a fabrication tolerance of only one part in $10^2$ could result in configuration-dependent delay variations of 3-5 cm.

We studied the problem of modeling the channel passbands for bandwidth synthesis. If the relative phases of the BWS channel local oscillators are known, but we have no auxiliary information about the phase shift in the filter, time delay errors on the order of 0.5 to 1 m can result from these filters. The use of an assumed-perfect calibrator can provide the information needed about the RF filters to reduce this error source to below 1 cm, as well as providing a definition point for time delay if the local oscillator phases are unknown.

We are currently in the process of studying the problem of modeling the passbands with full band sampling. In this case, the information inherent in the data appears sufficient to develop the RF filter models to within about 7 cm without external calibration. The use of an assumed-perfect calibrator appears to reduce this error source to well below 1 cm. Details of these results should appear next issue.
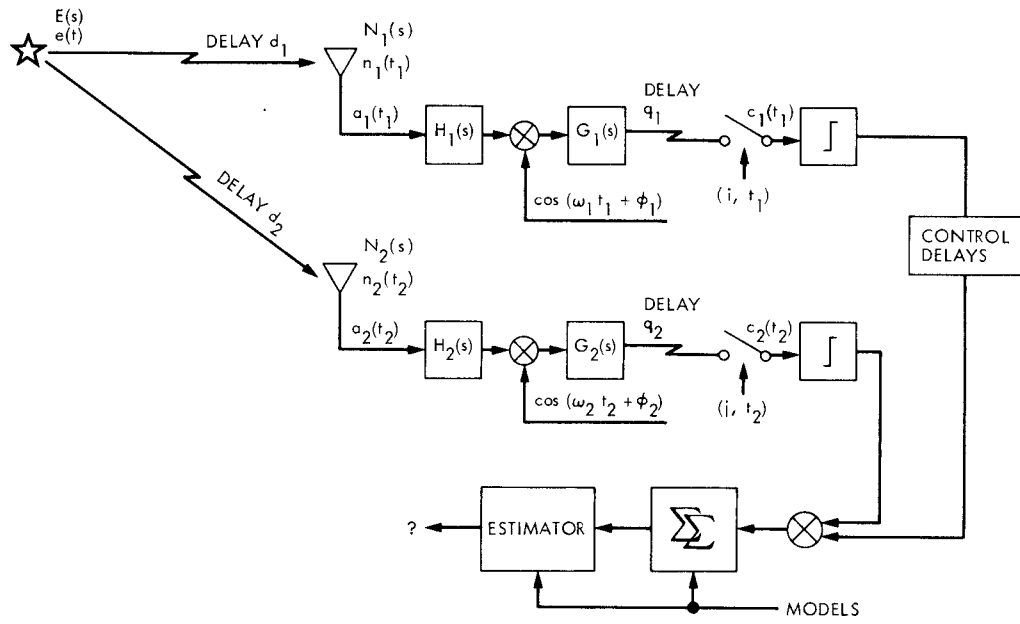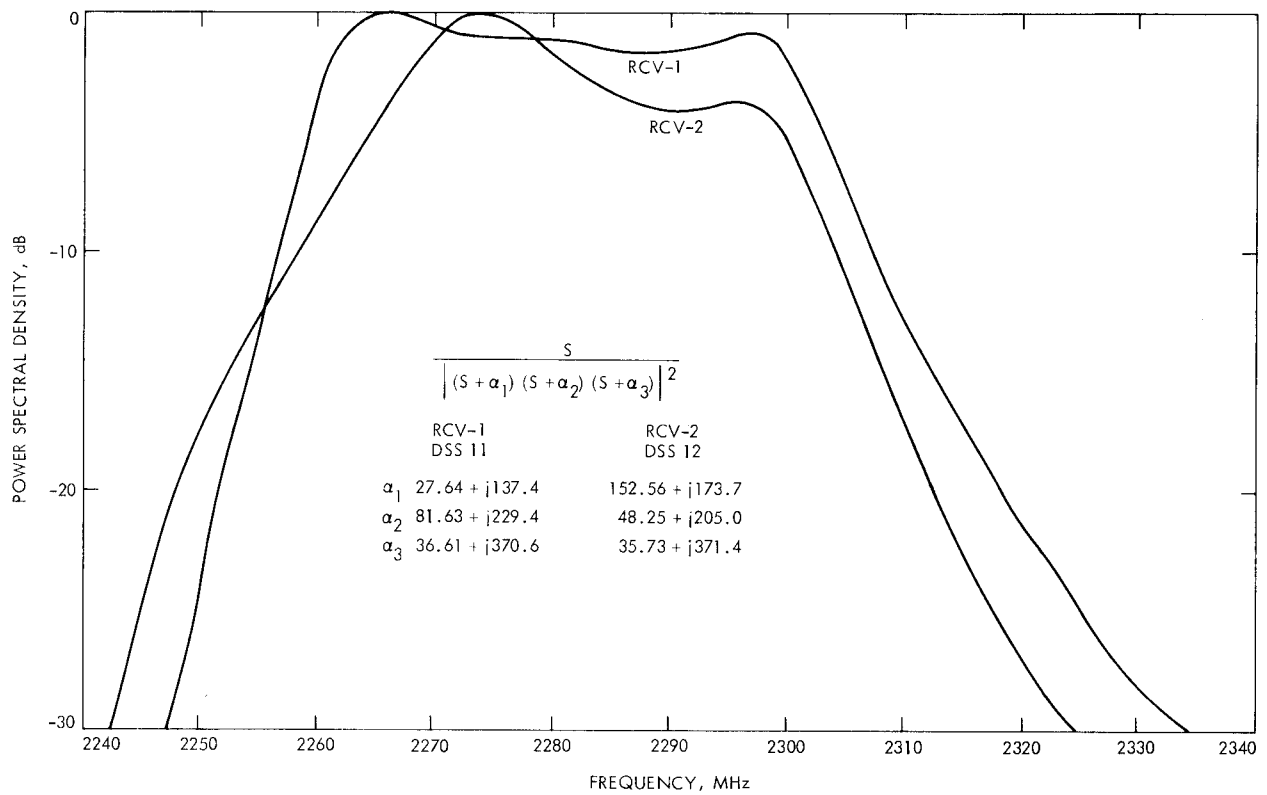
**Fig. 1 VLBI system block diagram**



$$\frac{S}{\left|(S+\alpha_1)\,(S+\alpha_2)\,(S+\alpha_3)\right|^2}$$

| | RCV-1<br>DSS 11 | RCV-2<br>DSS 12 |
|---|---|---|
| $\alpha_1$ | 27.64 + j137.4 | 152.56 + j173.7 |
| $\alpha_2$ | 81.63 + j229.4 | 48.25 + j205.0 |
| $\alpha_3$ | 36.61 + j370.6 | 35.73 + j371.4 |

**Fig. 2. Passbands of example RF filters**
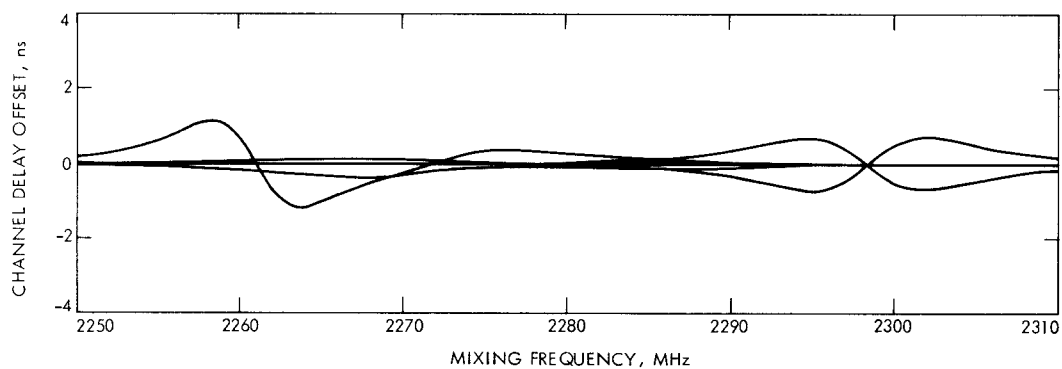
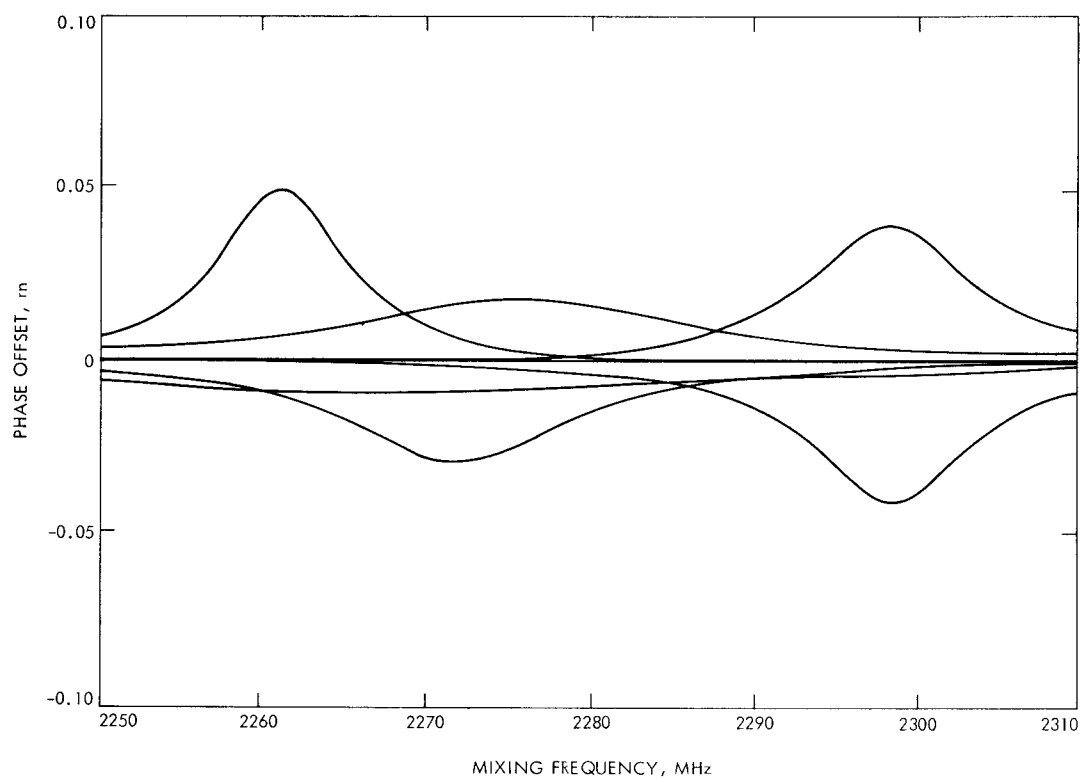**Fig. 3. Channel delay sensitivity to one part in $10^4$ change in RF filter poles**



**Fig. 4. Channel phase sensitivity to one part in $10^4$ change in RF filter poles**
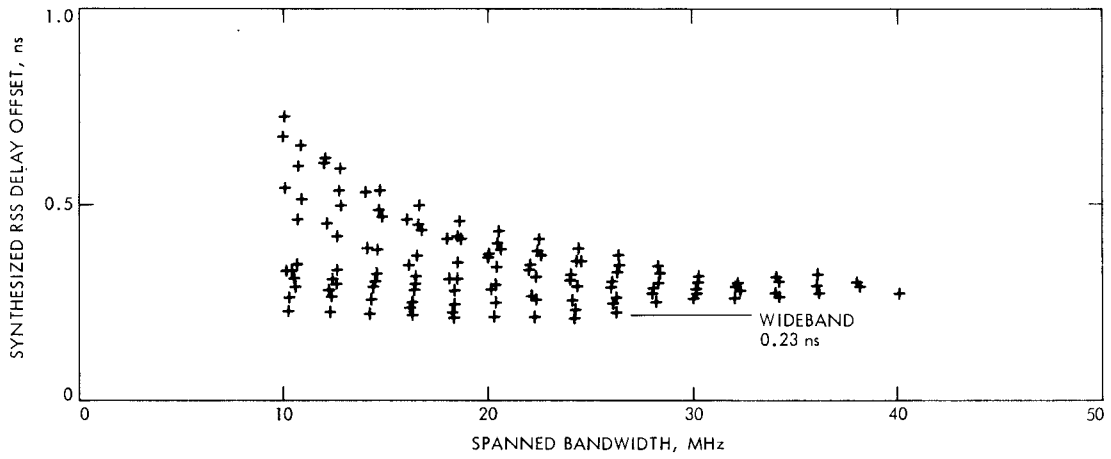
Fig. 5.  Total RSS delay sensitivity to one part in $10^4$ change in RF filter poles
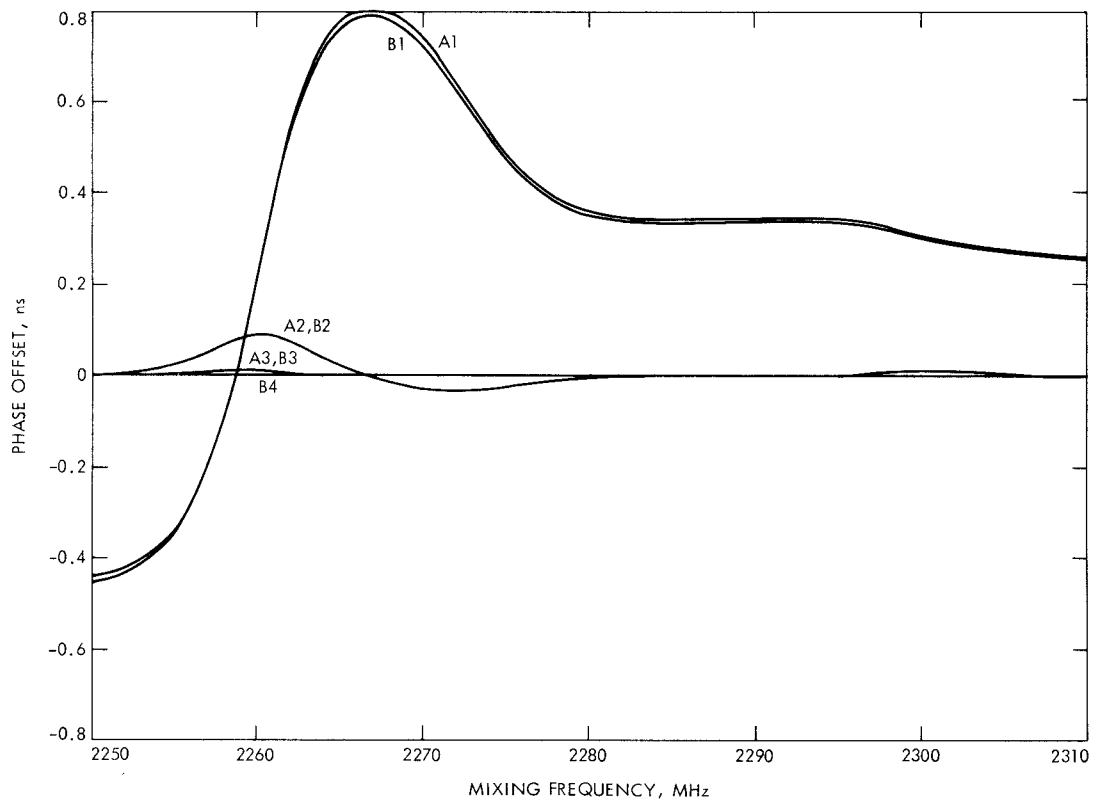


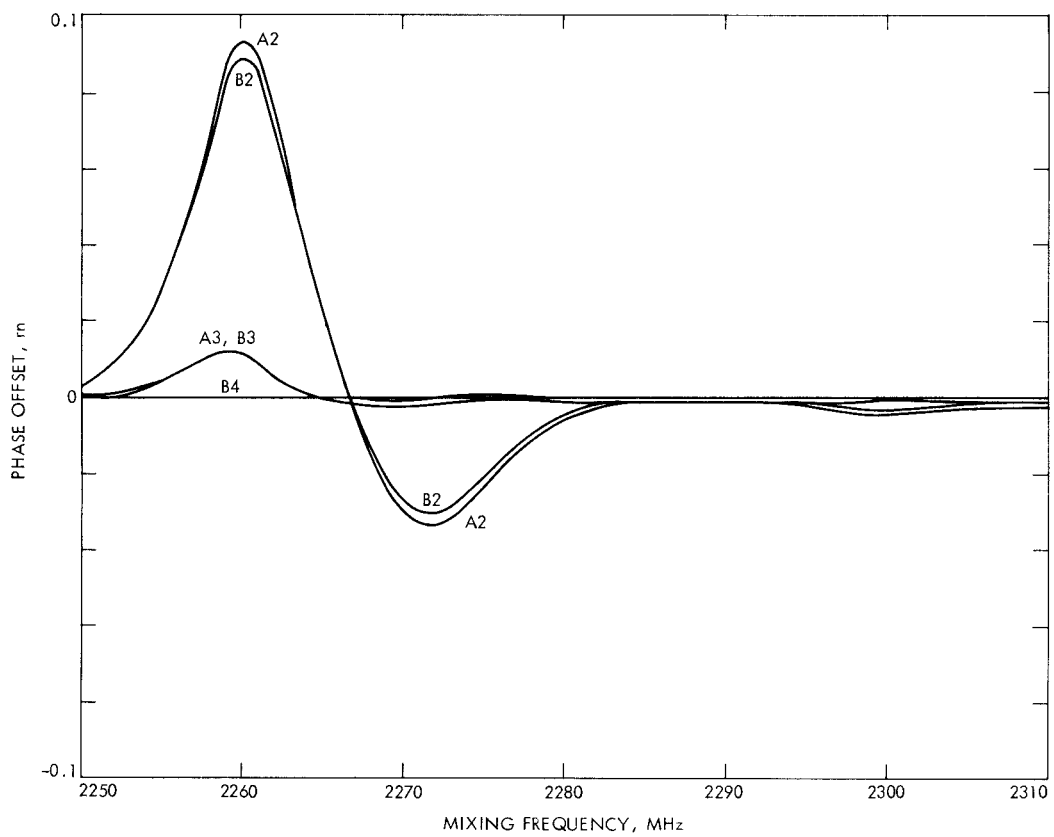Fig. 6.  Channel phase offset for channel models A1-A3, B1-B4, at $10^{-7}$ doppler

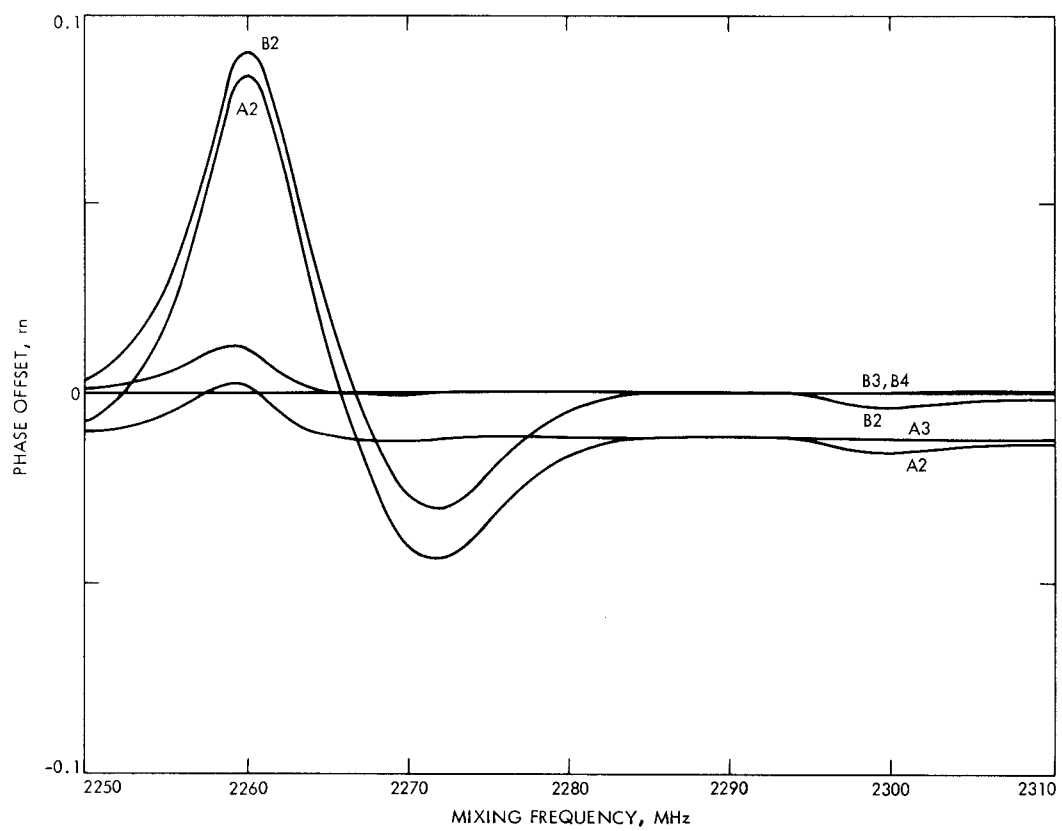**Fig. 7. Channel phase offset for channel models A2-A3, B2-B4, doppler = $10^{-7}$**
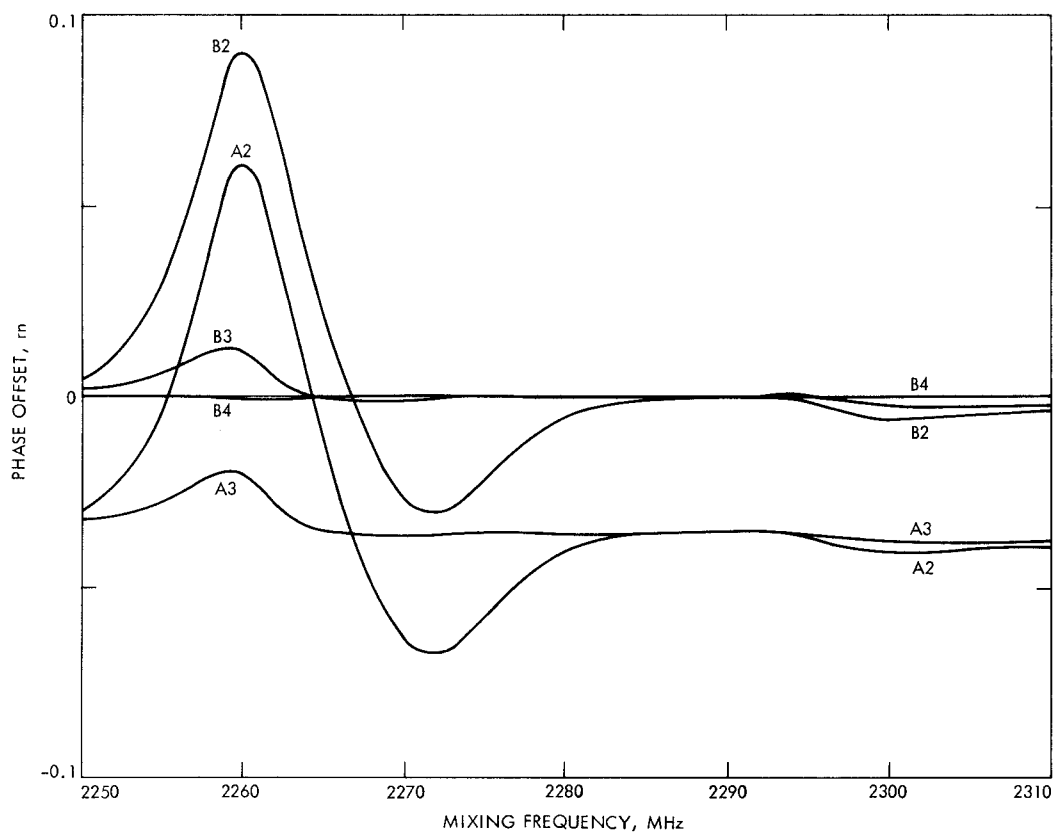
**Fig. 8. Channel phase offset for channel models A2-A3, B2-B4, doppler = $10^{-6}$**

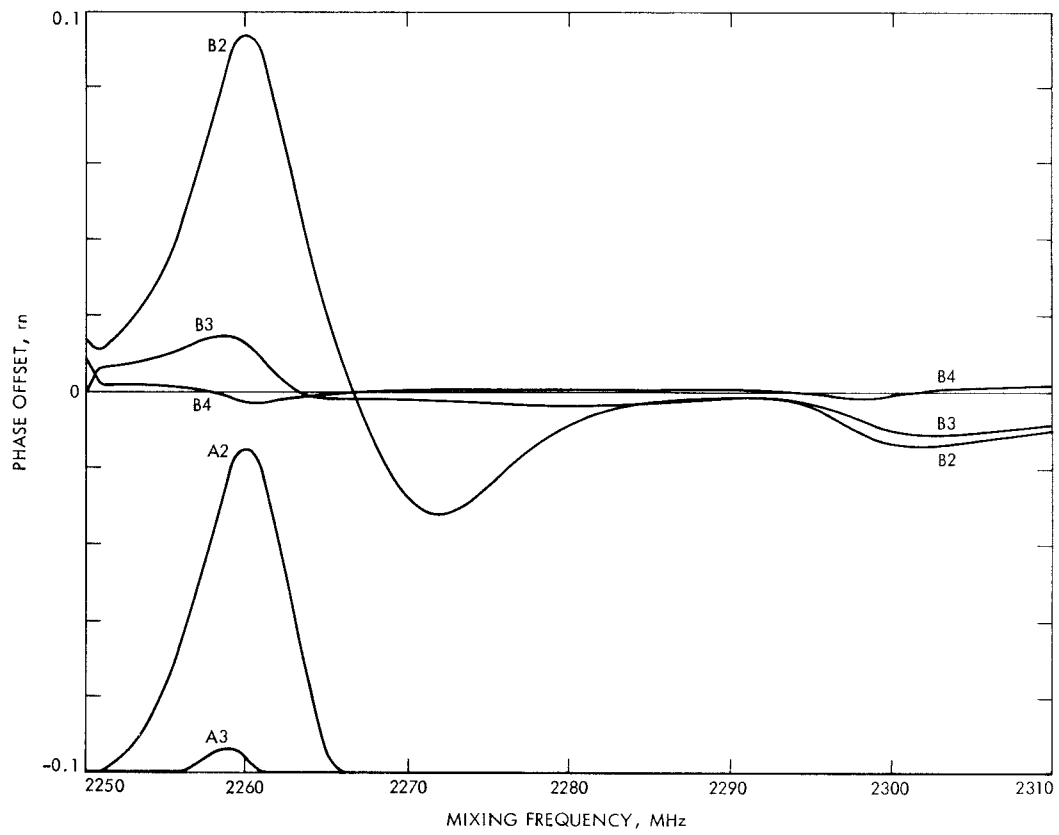Fig. 9. Channel phase offset for channel models A2-A3, B2-B4, doppler = $3 \times 10^{-6}$

PHASE OFFSET, rn

0.1

B2

B3

0

B4

B4

B3

A2

B2

A3

-0.1

2250  2260  2270  2280  2290  2300  2310

MIXING FREQUENCY, MHz

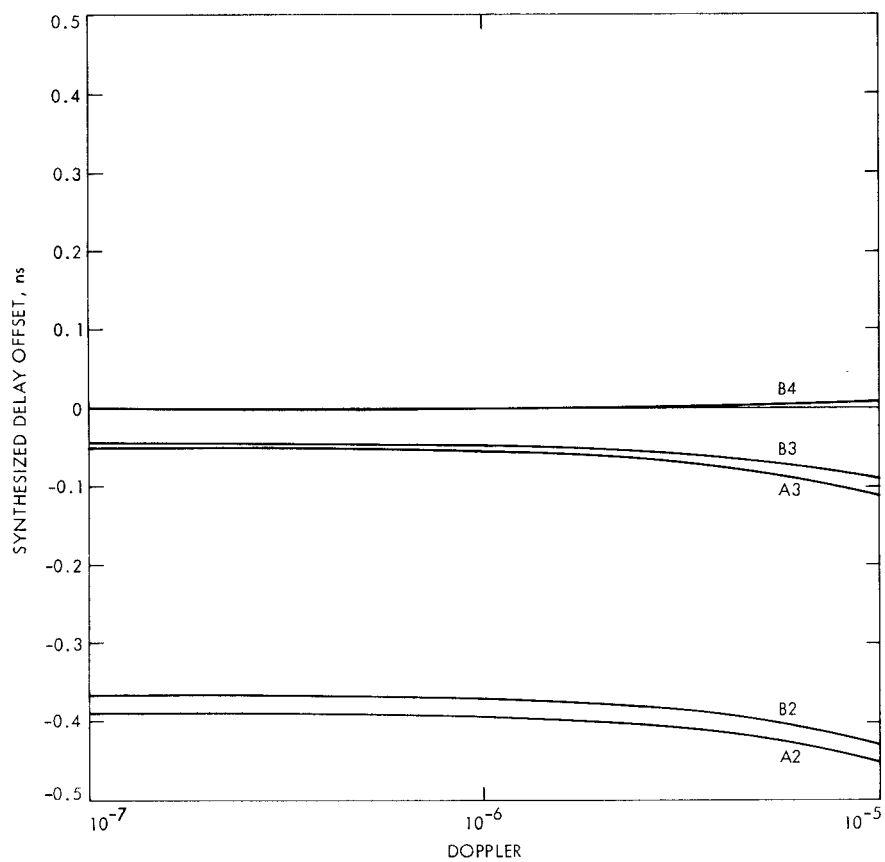**Fig. 10. Channel phase offset for channel models A2-A3, B2-B4, doppler = $10^{-5}$**

70

**Fig. 11. Synthesized delay offset as a function of doppler for channel models A2-A3, B2-B4**
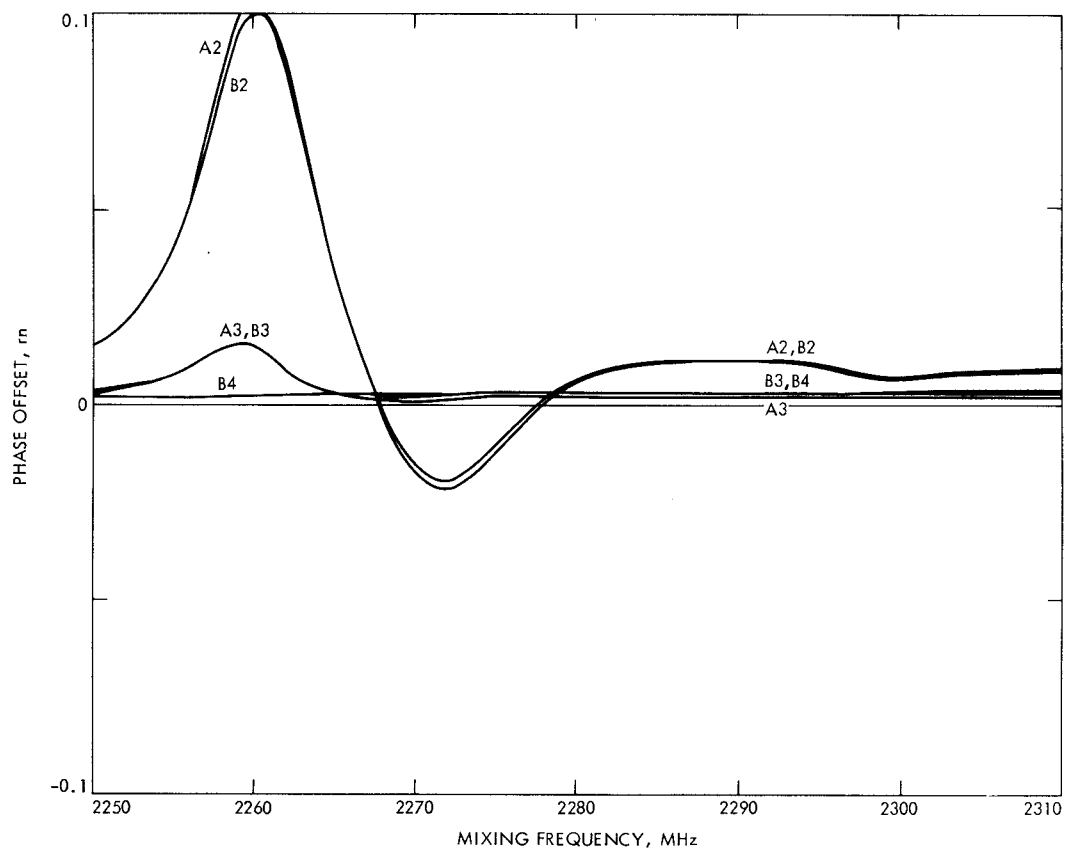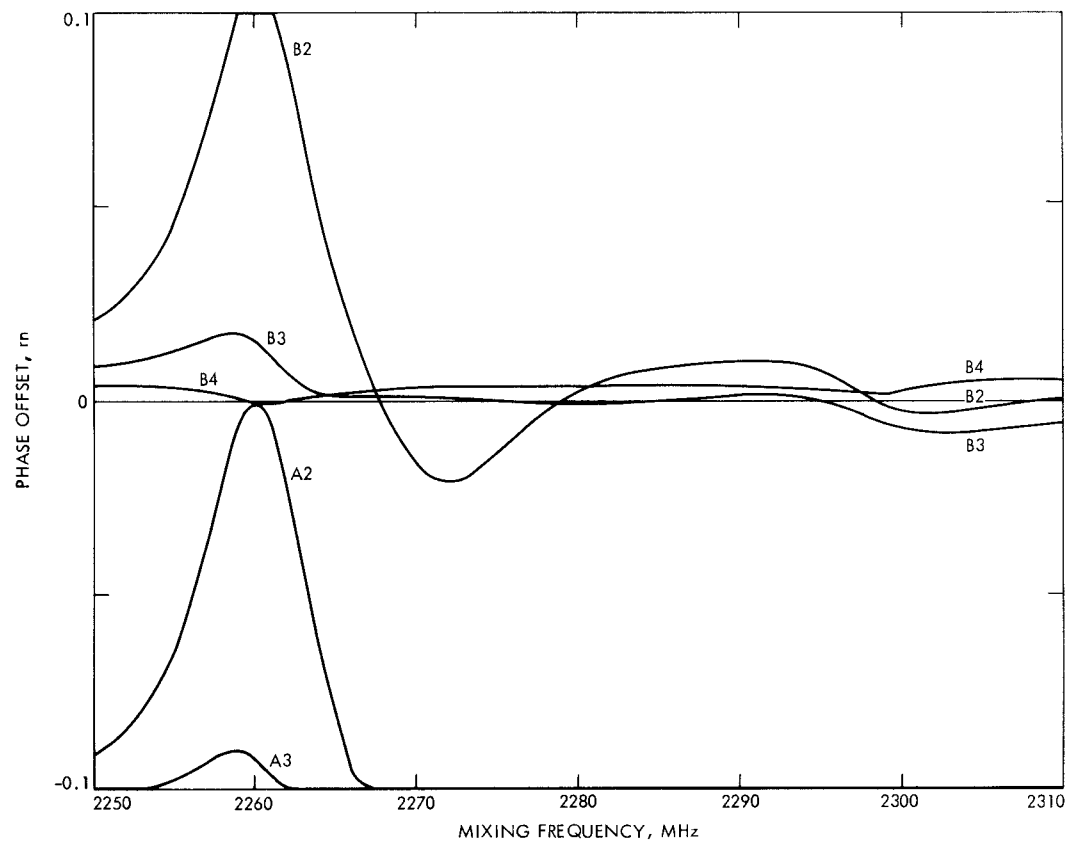
**Fig. 12. Channel phase offset with 10% mismatched final filter at receiver 1, for channel models A2-A3, B2-B4, doppler = $10^{-7}$**

**Fig. 13. Channel phase offset with 10% mismatched final filter at receiver 1, for channel models A2-A3, B2-B4, doppler = $10^{-5}$**

# Appendix A

## Expected Cross-Correlation Function
## For VLBI Samples

Let the input to the $i^{th}$ station sampler-limiter be expressed as in Eq. (11), i.e.,

$$c_i(t_i) = \int_{-\infty}^{t_i - q_i} g_i(t_i - q_i - \eta_i) \cdot \cos(\omega_i \cdot \eta_i + \phi_i)$$

$$\cdot \int_{-\infty}^{\eta_i} h_i(\eta_i - \xi_i) \qquad \text{(A-1)}$$

$$\cdot \left[ e(\xi_i - p_i - p_{i1} \cdot \xi_i) + n_i(\xi_i) \right] d\xi_i \, d\eta_i$$

where $g_i(\ )$, $h_i(\ )$ are impulse responses of the low-pass and RF filters, $q_i$ is the sampler delay, $\cos(\omega_i \cdot \eta_i + \phi_i)$ is the local oscillator mixing signal at time $\eta_i$, and $p_i - p_{i1} \cdot \xi_i$ is the locally linearized propagation delay at time $\xi_i$, near to $t_i$.

The cross-correlation function of the signals input to the station's sampler-limiters is defined by

$$R_c(t_1, t_2) = \langle c_1(t_1) \cdot c_2(t_2) \rangle \qquad \text{(A-2)}$$

where $\langle \cdot \rangle$ denotes ensemble average, and $c_1(t_1)$, $c_2(t_2)$ are as defined by Eq. (9). We will use the two-dimensional Fourier transform definitions of Papoulis (Ref. 13) to manipulate this function:

$$\Gamma_c(j\theta_1, j\theta_2) = \int dt_1 \int dt_2 \, e^{-j(\theta_1 t_1 - \theta_2 t_2)} R_c(t_1, t_2)$$

$$R_c(t_1, t_2) = \frac{1}{(2\pi)^2} \int d\theta_1 \int d\theta_2 \, e^{+j(\theta_1 t_1 - \theta_2 t_2)} \Gamma_c(j\theta_1, j\theta_2)$$

$$\text{(A-3)}$$

This form of the cross-correlation function is rapidly varying in both coordinates. It is convenient for calculations to change the coordinate system basis so that a form is obtained in which

rapid variation is suppressed in at least one coordinate. Thus define

$$S_c(t, \tau) = R_c(t, t + \tau) \qquad \text{(A-4)}$$

The transform of $S_c(\cdot, \cdot)$, by the definitions above, is

$$\psi_c(j\theta, j\eta) = \int dt \int d\tau \, e^{-j(\theta t - \eta \tau)} S_c(t, \tau)$$

$$= \Gamma_c(j\theta + j\eta, j\eta) \qquad \text{(A-5)}$$

It is of use to calculate $R_a(\cdot, \cdot)$ the correlation function and its transform at the input to the two receiving systems. The signal $e(t)$ is a white-noise process of density $N_e$ when it leaves its source. The signals $n_1(t_1)$ and $n_2(t_2)$ are independent white noise processes of densities $N_1$ and $N_2$. The desired correlation and its Fourier transforms are

$$R_a(t_1, t_2) = \langle \{ n_1(t_1) + e[t_1 \cdot (1 - p_{11}) - p_1] \}$$

$$\cdot \{ n_2(t_2) + e[t_2 \cdot (1 - p_{21}) - p_2] \} \rangle$$

$$= \frac{N_e}{2} \, \delta[t_1(1 - p_{11}) - p_1 - t_2(1 - p_{21}) + p_2]$$

$$\text{(A-6)}$$

$$\Gamma_a(j\theta_1, j\theta_2) = N_e \cdot \pi \cdot \frac{1}{1 - p_{11}} e^{-j\theta_1 \frac{p_1 - p_2}{1 - p_{11}}}$$

$$\delta \left( \theta_1 \frac{1 - p_{21}}{1 - p_{11}} - \theta_2 \right) \qquad \text{(A-7)}$$

These Fourier transforms will be extended by analytic continuation to become LaPlace transforms on the complex $s$-plane for manipulation of the filter functions. Inversion of the extended transform is via integration along the '$j\omega$' axis, since no poles in a physically realizable filter function will fall in the right-half-plane, or on the '$j\omega$' axis.

Having completed these preparations, we are now able to grind through the tedious, but not difficult, derivation of $S_c(\cdot\,,\cdot)$. From Eq. (9), we can write by inspection the LaPlace transforms $C_i(s_i)$ at the limiter-sampler inputs:

$$C_i(s_i) = e^{-q_i s_i} \cdot G_i(s_i) \cdot \frac{1}{2} \left[ e^{-j\phi_i} H_i(s_i + j\omega_i) \cdot A_i(s_i + j\omega_i) \right.$$

$$\left. + e^{+j\phi_i} H_i(s_i - j\omega_i) \cdot A_i(s_i - j\omega_i) \right] \qquad (A\text{-}8)$$

for $i = 1, 2$, where $A_i(s_i)$ is the LaPlace transform of $a_i(t_i)$. Likewise, we can write the product of $c_1(t_1)$ and $c_2(t_2)$, take their expected value, and LaPlace transform in two dimensions to obtain

$$\Gamma_c(s_1, s_2) = e^{-q_1 s_1} G_1(s_1) e^{+q_1 s_2} G_2(-s_2) \cdot \frac{1}{4}$$

$$\cdot \left[ e^{-j\phi_1} H_1(s_1 + j\omega_1) \Gamma_a(s_1 + j\omega_1, s_2 - j\omega_2) \right.$$

$$H_2(-s_2 + j\omega_2) e^{-j\phi_2}$$

$$+ e^{-j\phi_1} H_1(s_1 + j\omega_1) \Gamma_a(s_1 + j\omega_1, s_2 + j\omega_2)$$

$$H_2(-s_2 - j\omega_2) e^{+j\phi_2}$$

$$+ e^{+j\phi_1} H_1(s_1 - j\omega_1) \Gamma_a(s_1 - j\omega_1, s_2 - j\omega_2)$$

$$H_2(-s_2 + j\omega_2) e^{-j\phi_2}$$

$$+ e^{+j\phi_1} H_1(s_1 - j\omega_1) \Gamma_a(s_1 - j\omega_1, s_2 + j\omega_2)$$

$$\left. H_2(-s_2 - j\omega_2) e^{+j\phi_2} \right] \qquad (A\text{-}9)$$

It should be noted that for any systems we are likely to build, $G_i(s_i)$ are at least zonal low-pass, so that their response to frequencies greater than $\omega_i$ is negligible. Also, we expect $\omega_1 \approx \omega_2$, and from Eq. (A-7) we know that $\Gamma_a(j\theta_1, j\theta_2)$ is zero unless $\theta_1 \approx \theta_2$. These facts combine to make the first and fourth terms of the parenthesized factor in Eq. (A-9) identically zero, which helps to simplify our succeeding algebra.

When rotated into the desired coordinates, the transformed cross-correlation becomes

$$\psi_c(\theta, \eta) = e^{-q_1(\theta + \eta)} G_1(\theta + \eta) e^{q_2 \eta} G_2(-\eta) \cdot \frac{1}{4}$$

$$\cdot \left[ e^{-j\phi_1} H_1(\theta + \eta + j\omega_1) \right.$$

$$\Gamma_a(\theta + \eta + j\omega_1, \eta + j\omega_2) H_2(-\eta - j\omega_2) e^{+j\phi_2}$$

$$+ e^{+j\phi_1} H_1(\theta + \eta - j\omega_2) \Gamma_a(\theta + \eta - j\omega_1, \eta - j\omega_2)$$

$$\left. H_2(-\eta + j\omega_2) e^{-j\phi_2} \right] \qquad (A\text{-}10)$$

We now define the partially-inverse LaPlace transform of $\psi_c(\cdot\,,\cdot)$ with respect to its first argument as

$$\psi_c^*(t, \eta) = \frac{1}{2\pi j} \int_{-j\infty}^{+j\infty} e^{\theta t} \, \psi_c(\theta, \eta) d\theta \qquad (A\text{-}11)$$

To evaluate this integral, we insert the definition of $\Gamma_a(\cdot\,,\cdot)$ into Eq. (A-10) where the factors $\Gamma_a(\theta + \eta \pm j\omega_1, \eta \pm j\omega_2)$ are obtained by substituting $\theta + \eta \pm j\omega_1$ for $j\theta_1$, and $\eta \pm j\omega_2$ for $j\theta_2$ in Eq. (A-7), where the sign affixed to the mixing frequency is determined from the term selected in Eq. (A-10). We integrate by using the definition of the delta function — that its integral with respect to its argument has value unity, and that the entirety of this integral arises where the argument itself is zero, i.e., at

$$\eta \pm j\omega_2 = (\theta + \eta \pm j\omega_1) \frac{1 - p_{21}}{1 - p_{11}} \qquad (A\text{-}12)$$

or

$$\theta = \pm j(\omega_2 - \omega_1) + (\eta \pm j\omega_2) \left( \frac{p_{21} - p_{11}}{1 - p_{21}} \right) \quad (A\text{-}13)$$

By collecting terms, this integral becomes

$$\psi_c^*(t, \eta) = \frac{N_e}{8} \cdot \frac{1}{1 - p_{21}} \cdot e^{\eta \left( q_2 - q_1 \frac{1 - p_{11}}{1 - p_{21}} \right)} \cdot G_2(-\eta)$$

$$\cdot \left\{ e^{-j(\omega_2 t + \phi_2 - \omega_1 t - \phi_1)} \right.$$

$$\cdot e^{jq_1 \left( \omega_2 \frac{1-p_{11}}{1-p_{21}} - \omega_1 \right)}$$

$$\cdot e^{-(\eta - j\omega_2) \left( \frac{p_1 - p_2}{1-p_{21}} + t \frac{p_{11}-p_{21}}{1-p_{21}} \right)}$$

$$\cdot H_2(-\eta + j\omega_2) \cdot H_1 \left( (\eta - j\omega_2) \frac{1-p_{11}}{1-p_{21}} \right)$$

$$\cdot G_1 \left( (\eta - j\omega_2) \frac{1-p_{11}}{1-p_{21}} + j\omega_1 \right)$$

$$+ e^{+j(\omega_2 t + \phi_2 - \omega_1 t - \phi_1)}$$

$$\cdot e^{-jq_1 \left( \omega_2 \frac{1-p_{11}}{1-p_{21}} - \omega_1 \right)}$$

$$\cdot e^{-(\eta + j\omega_2) \left( \frac{p_1 - p_2}{1-p_{21}} + t \frac{p_{11}-p_{21}}{1-p_{21}} \right)}$$

$$\cdot H_2(-\eta - j\omega_2) \cdot H_1 \left( (\eta + j\omega_2) \frac{1-p_{11}}{1-p_{21}} \right)$$

$$\cdot G_1 \left( (\eta + j\omega_2) \frac{1-p_{11}}{1-p_{21}} - j\omega_1 \right) \right\} \quad \text{(A-14)}$$

The two terms discarded from Eq. (A-10) could be developed in an identical fashion, should the receiver configuration warrant their inclusion.

The desired correlation function is developed from $\psi_c^*(t,\eta)$ by transforming on $\eta$:

$$S_c(t,\tau) = \frac{1}{2\pi j} \int_{-j\infty}^{+j\infty} e^{-\eta\tau} \, \psi_c^*(t, \eta) \, d\eta. \quad \text{(A-15)}$$

We can simplify the appearance of the following equations by inserting the auxiliary variables $\phi_3$ and $\tau_3$ which are themselves functions of $t$ and $\tau$.

$$\tau_3 = \tau + q_1 \frac{1-p_{11}}{1-p_{21}} - q_2 + \frac{p_1 - p_2}{1-p_{21}} + t \frac{p_{11} - p_{21}}{1-p_{21}}$$

$$\phi_3 = \omega_2 t + \phi_2 - \omega_1 t - \phi_1 - \omega_2 \left( \frac{p_1 - p_2}{1-p_{21}} + t \frac{p_{11} - p_{21}}{1-p_{21}} \right)$$

$$- q_1 \left( \omega_2 \frac{1-p_{11}}{1-p_{21}} - \omega_1 \right) \quad \text{(A-16)}$$

This makes

$$S_c(\tau_3, \phi_3 : t, \tau) = \frac{N_e}{8} \cdot \frac{1}{1-p_{21}} \int_{-j\infty}^{+j\infty} \frac{d\eta}{2\pi j} e^{-\eta\tau_3} G_2(-\eta)$$

$$\cdot \left\{ e^{-j\phi_3} H_2(-\eta + j\omega_2) \right.$$

$$\cdot H_1 \left[ (\eta - j\omega_2) \frac{1-p_{11}}{1-p_{21}} \right]$$

$$\cdot G_1 \left[ (\eta - j\omega_2) \frac{1-p_{11}}{1-p_{21}} + j\omega_1 \right]$$

$$+ e^{+j\phi_3} H_2(-\eta - j\omega_2)$$

$$\cdot H_1 \left[ (\eta + j\omega_2) \frac{1-p_{11}}{1-p_{21}} \right]$$

$$\cdot G_1 \left[ (\eta + j\omega_2) \frac{1-p_{11}}{1-p_{21}} - j\omega_1 \right] \right\} \quad \text{(A-17)}$$

When the filters $G_i(s)$, $H_i(s)$ are expressed as rational polynomials in $s$, the integral in Eq. (A-17) is evaluated via the Heaviside expansion theorem into a sum of exponentials in $\eta\tau_3$ evaluated at the poles of $G_i(s)$, $H_i(s)$. If $\tau_3 < 0$, the integral is a normal inverse LaPlace integral, for which the selected poles are in the left-half plane, and are those of $G_1(s)$, $H_1(s)$. If $\tau_3 > 0$, the integral is an inverse LaPlace integral for *negative* time, which selects poles in the *right*-half plane, namely, those of $G_2(-s)$, $H_2(-s)$.

The autocorrelation of either $c_1(t_1)$ or $c_2(t_2)$ can be written by inspection from the cross-correlation

$$A_{ci}(t,\tau) = \frac{N_i + N_e}{8} \int_{-j\infty}^{+j\infty} \frac{d\eta}{2\pi j} e^{-\eta\tau}$$

$$[G_i(-\eta)H_i(-\eta + j\omega_i)H_i(\eta - j\omega_i)G_i(\eta)$$

$$+ G_i(-\eta)H_i(-\eta - j\omega_i)H_i(\eta + j\omega_i)G_i(\eta)] \quad \text{(A-18)}$$

The autocorrelations will be used in computing the cross-correlation at the output of the limiters.

Let $x$, $y$ be two gaussian random variables, and let $L(x)$ denote the limiter function that is $-1$ if $x < 0$, and $+1$ otherwise. Then it is easy to establish that

$$\langle L(x) \cdot L(y) \rangle = \langle L(x \cdot y) \rangle$$

$$= \frac{2}{\pi} \text{Arcsin}\left(\langle x \cdot y \rangle / \sqrt{\langle x \cdot x \rangle \cdot \langle y \cdot y \rangle}\right)$$

$$\text{(A-19)}$$

where $\langle \cdots \rangle$ denotes ensemble average. Note that $c_1(t_1)$ and $c_2(t_2)$ are gaussian random variables for any particular values of $t_1$, $t_2$, and hence Eq. (A-19) applies to the computation of the expected cross-correlation of the output of the limiters. In almost all cases of interest to VLBI, the correlated noise from the radio source is a very small part of the total noise at the receiver, i.e., $N_e \ll N_i + N_e$ for $i = 1$, or 2, so that a linear approximation to the Arcsin ($\cdot$) in Eq. (A-19) is adequate. Thus, if we denote as $S_L(\cdots)$ the cross-correlation of the limiter-output signals, then

$$S_L(\tau_3, \phi_3 : t, \tau) = \frac{2}{\pi} \frac{S_c(\tau_3, \phi_3 : t, \tau)}{\sqrt{A_{c1}(0,0) \cdot A_{c2}(0,)}} \quad \text{(A-20)}$$

The *variance* of each $S_L(\cdots)$ is unity, since the magnitude of $L(x)$ is identically one. The covariance of $S_L(\cdot \cdot : t, \tau)$ will be needed for SNR calculations.

# Appendix B

# Square Passband Filters

We can obtain at least a partial check on the derivation from Appendix A by reverting to the special case of square passbands with single-sideband demodulators, for which a simpler derivation is possible. Let

$$G_i(jx) = \begin{cases} 1 & \text{for } |x| < \omega_1, \omega_2 \\ 0 & \text{elsewhere} \end{cases}$$

(B-1)

$$H_i(jx) = \begin{cases} 1 & \text{for } \omega_i < |x| < \omega_i + B_i \\ 0 & \text{elsewhere} \end{cases}$$

where $B_i$ is the bandwidth of the supposed square-passband filters. Denote by $S_{SQ}(\cdots)$ the form assumed by $S_c(\cdots)$ for this special case.

$$S_{SQ}(\tau_3,\phi_3:t,\tau) = \frac{N_e}{8} \cdot \frac{1}{1-p_{21}} \cdot \left\{ e^{+\phi_3} \int_{jb}^{jB} \frac{d\eta}{2\pi j} e^{-\eta\tau_3} \right.$$

$$\left. + e^{-\phi_3} \int_{-jB}^{-jb} \frac{a\eta}{2\pi j} e^{-\eta\tau_3} \right\}$$

(B-2)

where

$$b = \max \left\{ 0, \frac{1-p_{21}}{1-p_{11}}\omega_1 - \omega_2 \right\}$$

and

$$B = \min \left\{ B_2, \frac{1-p_{21}}{1-p_{11}}(\omega_1 + B_1) - \omega_2 \right\}$$

The execution of these integrals results in the anticipated $\sin(x)/x$ form; i.e.,

$$S_{SQ}(\tau_3,\phi_3:t,\tau) = \frac{N_e}{8} \cdot \frac{1}{1-p_{21}} \cdot \frac{1}{2\pi} \cdot \frac{1}{\tau_3} \cdot \sin\left(\frac{B-b}{2}\tau_3\right)$$

$$\cdot \cos\left(\frac{B+b}{2}\tau_3 - \phi_3\right)$$

(B-3)

Equation (B-3) describes a cross-correlation with a magnitude and phase factor. If we let $\phi_4$ be the argument of the phase factor, we can collect terms in $\phi_4$ to place it into the form:

$$\phi_4 = \frac{B+b}{2}\tau_3 - \phi_3$$

$$\phi_4 = \phi_x + t(\omega_1 - \omega_2) + \left(\omega_2 + \frac{B+b}{2}\right) \cdot \frac{p_{11} - p_{21}}{1-p_{21}} \cdot t$$

$$+ \frac{B+b}{2}\tau$$

(B-4)

where $\phi_x$ is an undetermined phase angle. This corresponds with the "fringe phase" of Thomas (Ref. 14), if $\omega_2 + (B+b)/2$ is interpreted as the "center of the doppler-shifted passband" at RF.

The autocorrelation of either receiver output is

$$A_{SQ_i}(t,\tau) = \frac{N_i + N_e}{2} \cdot \frac{1}{2\pi} \cdot \frac{\sin\left(\frac{B_i}{2}\tau\right)}{\tau} \cdot \cos\left(\frac{B_i}{2}\tau\right)$$

(B-5)

If we denote as $S_{LQ}(\cdots)$ the cross-correlation at the output of the limiters with square passband filters, and use Eq. (B-5) with the weak-signal approximation to Eq. (A-19),

$$S_{LQ}(\tau_3,d_3:t,\tau) = \frac{N_e}{\sqrt{N_1 N_2}} \cdot \frac{2/\pi}{1-p_{21}} \cdot \frac{\sin\left(\frac{B-b}{2}\tau_3\right)}{\frac{\sqrt{B_1 B_2}}{2} \cdot \tau_3}$$

$$\cdot \cos\left(\frac{B+b}{2}\tau_3 - \phi_3\right)$$

(B-6)

is the expected value of the cross-correlation function observed in VLBI processing.

# Acknowledgments

# References

1. Counselman, C. C. III, "Very-Long Baseline Interferometry Techniques Applied to Problems of Geodesy, Geophysics, Planetary Science, Astronomy, and General Relativity," *Proc. IEEE*, Vol. 61, No. 9, Sept. 1973, pp. 1225-1230.

2. Clauss, R., et al., "Low Noise Receivers: Microwave Maser Development," *DSN Progress Reports,* TR 32-1526, Vol. XI, Jet Propulsion Laboratory, Pasadena, Calif., Oct. 15, 1972, pp. 71-80.

3. Rogers, A. E. E., "Very Long Baseline Interferometry with Large Effective Bandwidth for Phase-Delay Measurements," *Radio Sci.,* Vol. 5, No. 10, Oct. 1970, pp. 1239-1247.

4. Hurd, W. J., "DSN Clock Synchronization by Maximum Likelihood VLBI," *DSN Progress Report* TR 32-1526, VOL X, Jet Propulsion Laboratory, Pasadena, Calif., Aug. 15, 1972, pp. 82-95.

5. Barankin, E. W., "Locally Best Unbiased Estimates," *Ann Math Stat.*, Vol. 20, 1949, pp. 477-501.

6. Cramer, H., *Mathematical Methods of Statistics*, Princeton Univ. Press, 1945.

7. Hurd, W. J., "Preliminary Demonstration of Precision DSN Clock Synchronization by Radio Interferometry," *DSN Progress Report 42-37*, Feb. 15, 1977, pp. 57-68.

8. Rogers, A. E. E., et al., "Very Long Baseline Interferometry Hardware," Final Report for Contract NAS5-20777, Feb. 1976, Part 7, "An IF to Video Converter", Haystack Technical Note 1975-5.

9. Weaver, D. K., "Design of RC Wide-Band 90-Degree Phase-Difference Network," *IRE Proc.*, Apr 1954, pp. 671-676.

10. Urech, J. M., et al., "S-Band Maser Group Delay Measurements and Stability Report," Madrid Deep Space Station, Oct. 1976.

11. Rogers, A. E. E., et al., "Very Long Baseline Interferometry Hardware," Final Report for Contract #NAS5-20777, Feb. 1976, Part 13 "A Receiver Phase and Group Delay Calibration System", Haystack Technical Note 1975-6.

12. Thomas, J. B., "The Tone Generator and Instrumental Calibrations in VLBI Measurements," JPL Internal Report EM-315-31, July 15, 1977.

13. Papoulis, A., *Probability, Random Variables, and Stochastic Processes,* Sec. 12-2, McGraw-Hill Book Company, New York, 1965.

14. Thomas, J. B., "System Noise Effects in VLBI Measurements," JPL Internal Report EM 315.6, Oct. 25, 1976.

**Table 1. Offset in estimated group delay and phase for $1_{10}-4$ offset in filter pole position with full band sampling**

| Pole no. | | $\Delta$ delay, ns | $\Delta$ phase, rn |
|---|---|---|---|
| 1a | | −0.099 | 0.0067 |
| 1b | | −0.027 | 0.0135 |
| 1c | | 0.124 | 0.0079 |
| 2a | | 0.032 | −0.0068 |
| 2b | | 0.099 | −0.0130 |
| 2c | | −0.132 | −0.0081 |
| | RSS (all) | 0.23 | 0.024 |


**Table 2. Change in estimated channel phase for $1_{10}-2$ change in final filter pole position. (Rn $\times 10^{-3}$)**

| Pole | Phase at 2260 | Phase at 2300 | $|\Delta\phi|$ |
|---|---|---|---|
| 1a | 3.34 | 3.18 | 0.16 |
| 1b | 5.07 | 4.66 | 0.41 |
| 1c | 1.91 | 1.90 | 0.01 |
| 1d | 1.27 | 0.80 | 0.47 |
| 1e | 6.71 | 6.33 | 0.38 |
| 1f | −1.62 | −1.74 | 0.12 |
| 1g | 11.2 | 9.13 | 2.1 |
| 2a | −3.65 | −3.17 | 0.48 |
| 2b | −5.45 | −4.65 | 0.80 |
| 2c | −2.15 | −1.89 | 0.26 |
| 2d | −1.12 | −0.80 | 0.32 |
| 2e | −7.47 | −6.30 | 1.17 |
| 2f | 2.15 | 1.72 | 0.43 |
| 2g | −11.9 | −9.11 | 2.8 |
| RSS | 22.2 | 18.0 | 3.6 |


**Table 3. Change in estimated channel phase for $1_{10}-2$ change in quad-hybrid filter pole positions (rn $\times 10^{-3}$)**

| Pole | Phase at 2260 | Phase at 2300 | $|\Delta\phi|$ |
|---|---|---|---|
| 1a | 0.323 | 0.405 | 0.08 |
| 1b | 1.69 | 1.82 | 0.13 |
| 1c | 1.07 | 1.31 | 0.28 |
| 1d | 1.79 | 1.73 | 0.06 |
| 2a | −0.376 | −0.404 | 0.03 |
| 2b | −1.92 | −1.81 | 0.11 |
| 2c | −1.24 | −1.30 | 0.06 |
| 2d | −1.97 | −1.72 | 0.25 |
| RSS | 4.08 | 4.03 | 0.43 |